Her-Yueh Huang*, Chung-Wei Yang and Wen-Yao Deng

Incorporating oxygen-free copper to improve the microstructure and mechanical properties of friction-stir-welded joints for aluminum alloys

https://doi.org/10.1515/secm-2016-0241
Received August 14, 2016; accepted February 16, 2018; previously published online April 9, 2018

Abstract: The main objective of the present work was to establish a friction-stir-welding process to weld dissimilar metal joints on AA6082 and AA6066 aluminum alloy plates. Joints were made while varying tool rotation speed at a constant traveling speed and at the same time adding oxygen-free copper reinforcement inside the weld nugget for the purpose of analyzing the microstructural evolution and mechanical properties of the joint. Results showed that the morphology of the microstructure in the weld nugget changed significantly with rotation speed. Optical microscopy, scanning electron microscopy, and energy dispersive spectroscopy analyses revealed that oxygen-free copper particles could be uniformly dispersed into the weld nugget because of higher rotation speeds. Because of the presence of reinforcement particles homogenously distributed inside the nugget zone, the mechanical properties, such as ultimate tensile strength and hardness of weld joint, were greatly improved.

Keywords: dissimilar joints; friction stir welding; mechanical properties; microstructure; particle reinforcements.

1 Introduction

Aluminum and its alloys are lightweight, nonferrous metals with good corrosion resistance, ductility, and strength. These metals are also versatile with applications in almost every industrial and commercial segment [1–3]. Aluminum also offers many other advantages because of its material properties. Aluminum is relatively easy to use in fabrication and machining processes. As more and more main structural parts and components are produced from aluminum, its use in welding will inevitably increase in industry [4]. In many instances, with conventional fusion welding techniques, problems are caused by the occurrence of heat-affected zone softening, solidification cracking, and residual stresses. To overcome these issues, friction stir welding (FSW), a relatively new solid-state joining technique, seems to be a promising method [5–8].

In the FSW process, a hard tool, generally consisting of a shoulder and a pin, is forced into the workpieces, generating frictional heat between the tool and the workpiece. This creates local softening of materials and improves the plasticized material flow around the pin resulting in a significant grain refinement within the nugget zone [2]. However, the FSW of similar or dissimilar metals can produce good quality joints while maintaining the desired mechanical properties. Some research has indicated that reinforcing material in the FSW process improves the properties of welds, making them superior to ordinary FSW welds. For example, in some studies a groove filled with microscale and nanoscale particles directly reinforced the weld nugget through FSW [9–12]. Another method used was a thin metal foil as reinforcement between the faying surfaces of the weld [13–15]. Most of the above used metallography observation, tensile testing, hardness, failure analysis, and so on. For the structure construction, reinforcement that is uniformly distributed is vital. This implies that the different FSW process parameters of the welds lead to different material flow behaviors, such as rotational speed and traverse speed, and thus influence the microstructures and mechanical properties of the joint [16–18].

Based on the above, a dissimilar FSW for AA6082 and AA6066 aluminum alloy sheets was carried out, achieving a sound dissimilar joint applying appropriate welding parameters. To clarify the plastic flow of material in FSW joints, oxygen-free copper (OFC) not only was useful for its chemical purity but also made it possible to fabricate a joint exhibiting higher tensile strength. These OFC-reinforced particles provided good markers for the material flow, contributing to a better understanding of the role of the OFC in enhancing the mechanical properties. The

***Corresponding author: Her-Yueh Huang,** Department of Materials Science and Engineering, National Formosa University, Yunlin 632, Taiwan, Phone: +886 5 631 5479, Fax: +886 5 636 1981, e-mail: huanghy@nfu.edu.tw
Chung-Wei Yang: Department of Materials Science and Engineering, National Formosa University, Yunlin 632, Taiwan
Wen-Yao Deng: Graduate Institute of Materials Science and Green Energy Engineering, National Formosa University, Yunlin 632, Taiwan

rotation speeds of the tool were taken to be controllable parameters in the investigation of the reinforcement particle distribution in the weld nugget. In addition, detailed microstructural examination and characterization of the weld nugget were performed. The mechanical properties such as microhardness and tensile strength were also evaluated. Further, the influence of the reinforcement particle addition on the relationship between microstructure and mechanical properties was also established.

2 Materials and methods

This experiment used commercially produced AA6082 and AA6066 aluminum alloy plates with a thickness of 5 mm cut to 100 mm by 50 mm. The chemical compositions of the experimental materials are listed in Table 1. Before FSW, the surfaces of the plates were ground with grit paper to remove the oxide film and then cleaned with acetone. OFC foil (0.5 mm thick) with purity of more than 99.9% was used as reinforcement.

The configuration for the initial butt joint for fabricating the FSW joints was obtained by using mechanical clamps to secure the plates in position, as shown in Figure 1. The OFC foil was placed between the faying edges; the AA6082 plate was placed on the advancing side, and the AA6066 plate was placed on the retreating side. A standard steel (SKD61) tool was used for welding the aluminum alloy with a shoulder of 12 mm in diameter and a cylindrical pin 4 mm in diameter and 4.6 mm in length. The tool tilt in all the trials was kept constant at 2° to give sufficient stirring and the necessary compressive force to the weld zone. The tool rotation speeds used in this study were 1720 ($20\times g$), 2093 ($29\times g$), and 2896 rpm ($56\times g$), while the traverse speed was 30 mm/min.

Specimens for microstructure observation were cut perpendicular to the welding direction and then embedded in an epoxy resin. After a series of grinding and polishing processes, the surface of the specimens was etched with Keller's agent. The microstructural changes from the weld nugget to the unaffected base metal were examined with an optical microscope (DSX-HRSU, Olympus, Japan). Scanning electron microscopy (SEM) (SU3500, Hitachi, Japan) with the attachment of energy-dispersive X-ray spectroscopy (EDS) (QX-400, Bruker, Japan) was also used in order to examine the more delicate structures formed in the weld nugget. The FSW samples and base metals were analyzed using X-ray diffraction (XRD) (D8 Advance, Bruker, Germany) to identify the phases in the materials.

The Vickers hardness profile of the weld zone was measured on the cross section perpendicular to the welding direction using an indentor with a load of 100 gf for a dwell period of 20 s while data were taken from several locations in the top, middle, and bottom layers. The room temperature tensile tests were performed using a universal tensile test machine operated at a constant crosshead speed with an initial strain rate of 0.001 mm/s. After tensile testing, the fracture surface characteristics

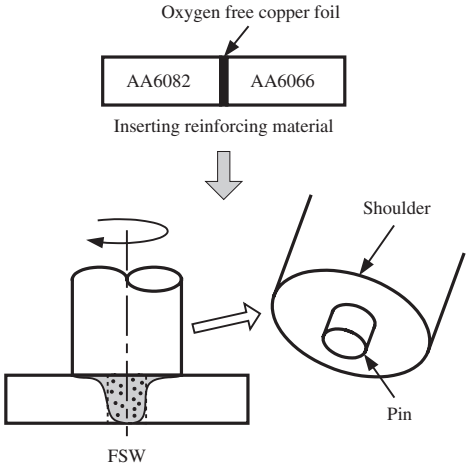

Figure 1: Schematic illustration of the friction-stir butt welding process.

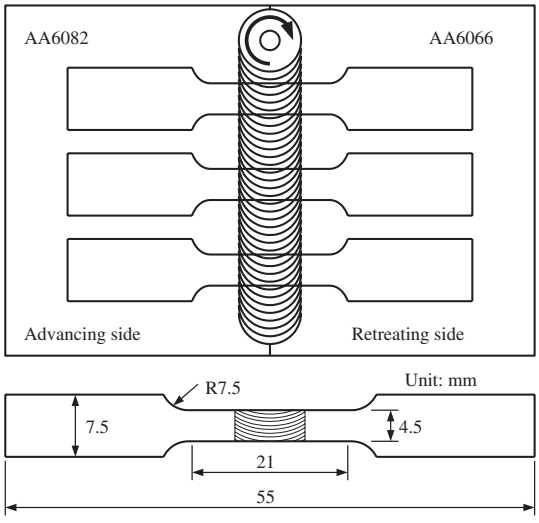

Figure 2: Dimension and locations of the tensile specimen sampling in dissimilar metal weldments.

Table 1: Compositional analysis (in weight percent) of the experimental materials.

Alloy	Si	Fe	Cu	Mn	Mg	Zn	Ti	Cr	Al
6082	1.16	0.24	0.07	0.64	0.99	0.03	0.03	0.16	Bal.
6066	1.36	0.17	1	1.04	0.99	0.04	0.02	0.17	Bal.

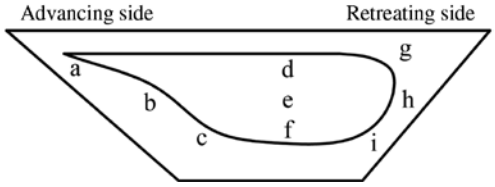

Figure 3: Schematic illustration of the sampling position for the microstructure analysis in Figures 4–6.

of the specimens were examined by SEM. The shape and dimensions of the tensile test specimen are shown in Figure 2. The surfaces of the specimen were polished with 400 grit silicon carbide paper before the tensile test.

3 Results and discussion

3.1 Microstructure of joints

The cross-sectional microstructures perpendicular to the welding direction in the friction stir with dissimilar butt joints, under different rotation speeds, are shown in Figures 3–6. In the cross section, the left- and right-hand sides of the weld center were consistent with the advancing and retreating sides of the rotating tool, respectively. Figure 4 shows the weld nugget exhibiting a high degree of continuity and no defects at the rotation rate of 2896 rpm. Micrographs of the welds showed a typical stir zone ("nugget"), thermo-mechanically affected zone and heat-affected zone. The nugget could be easily identified as the "onion-ring" structure was mainly visible on the center of the nugget (Figure 4E). The material in this region had undergone the most severe plastic deformation during FSW. A banded zone appeared in the top portion of the shoulder flow zone as well as the weld nugget zone (Figure 4A,B), similar to the banded zone aggregates on the advancing side. However, the chemical composition of the banded zone had not changed. A possible explanation for the banded zone could be the complex material flow occurring during FSW. This zone exhibited poor plastic flow of the metal and caused some large OFC fragmentation in the nugget zone. As can also be seen, there was significant breakup of OFC particles, consequently presenting

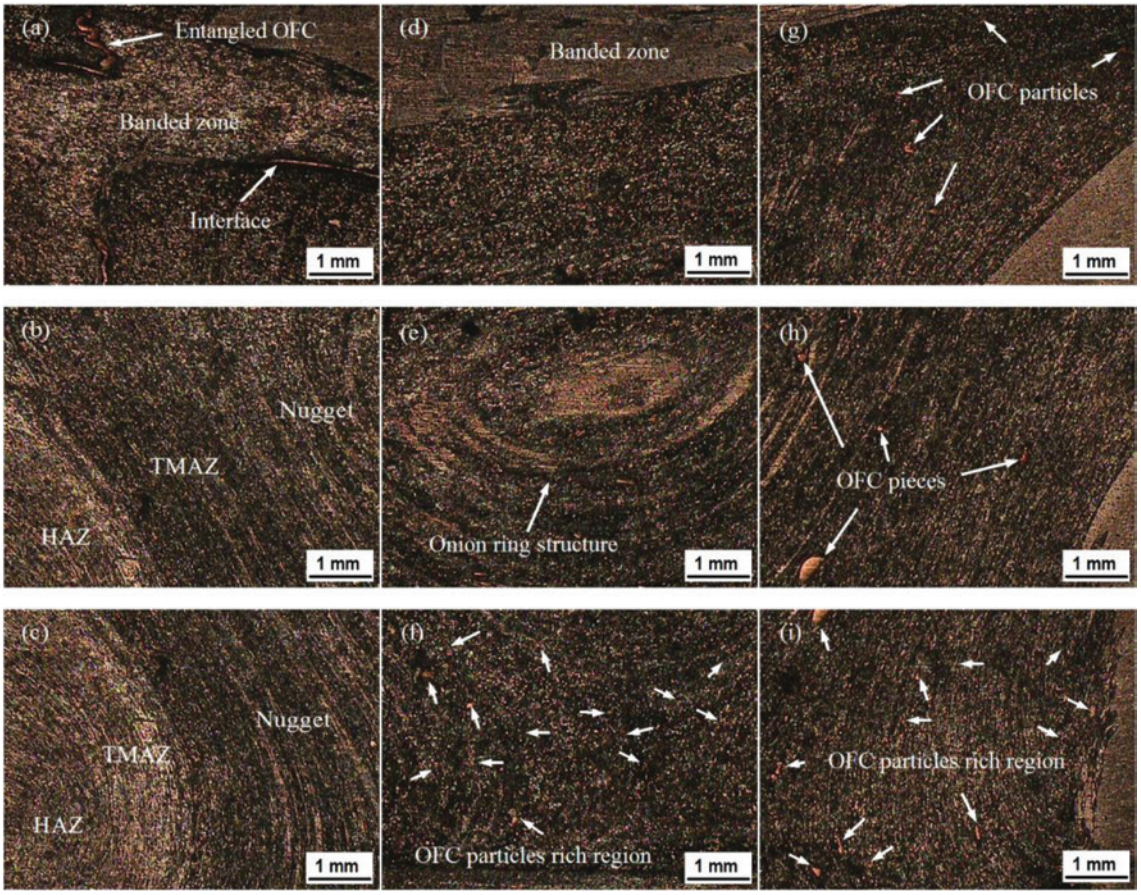

Figure 4: Optical microscope images taken from the cross section of different areas in dissimilar metal butt joints at a rotation speed of 2896 rpm. (a) to (i) Indicates sampling locations as shown in Figure 3.

a uniform distribution in the center weld nugget region and the retreating side. This was because material flows mainly occurred on the retreating side and the dragging of the plasticized material behind the tool formed the welded joint. Therefore, only few OFC particles were observed on the top advancing side in the upper midsection.

The joint welded at lower rotation speed, 2083 rpm, resulted in weld defects as shown in Figure 5. A cluster of voids in the center weld nugget region and the advancing side of the weld were identified. Furthermore, cavities filled with copper fragments were found on the advancing side of the weld nugget, thus revealing the weld had defects formed because of weak intermixing between the aluminum alloy and OFC. Generally, the onion rings found in the nugget were evidence of proper plastic flow occurring during FSW. The reduced stirring due to the lower rotation speed retarded the flowability of the plastic material, which may have caused the onion ring structure not being completely formed at rotational speed of 2083 rpm.

The samples welded at tool rotation speed of 1720 rpm formed a large number of cavities in the nugget (Figure 6). Such cavity defects are generally formed outside the optimum parameters as a result of insufficient frictional heating of the joint when low tool rotation speed was applied. In terms of weld quality, although the central weld nugget of all welds contained OFC fragmentation, those at the lowest tool rotational speed (1720 rpm) were bigger accompanied by a large number of voids. Besides, a crack initiated on the retreating side at the interface between the weld nugget and the thermo-mechanically affected zone was also observed, which might have led to a lower tensile strength.

Based on the experimental results shown in Figures 4–6, the effect of rotation speed on the weld microstructure could be summarized. Rotation speed contributed to the formation of various microstructures in the weld nuggets. It also determined the heat input and plastic flow and in turn influenced the quality of weld joints. Essentially, as rotation speed increased, the material flow dynamic changed and appeared to have become more fluid, similar to that in 2896 rpm. With less banded structure and onion ring formation, the OFC particles

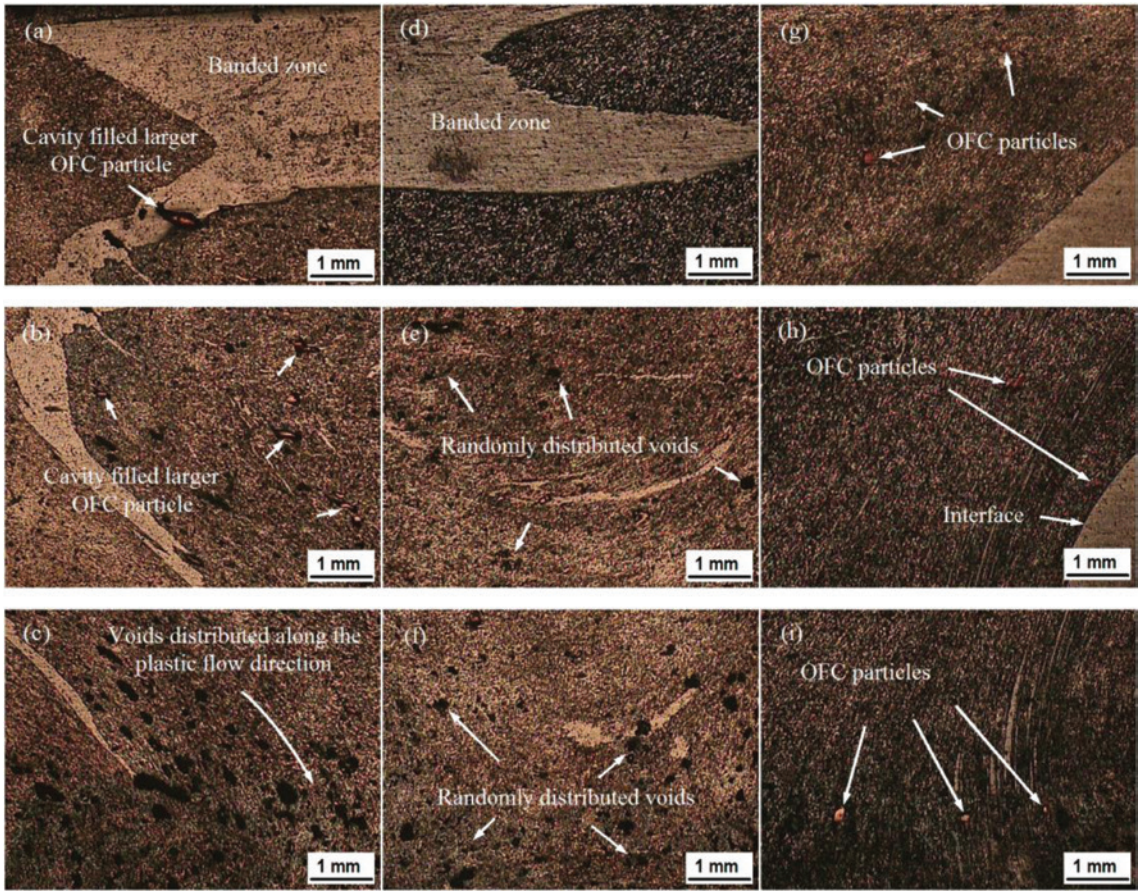

Figure 5: Optical microscope images taken from the cross section of different areas in dissimilar metal butt joints at a rotation speed of 2093 rpm. (a) to (i) Indicates sampling locations as shown in Figure 3.

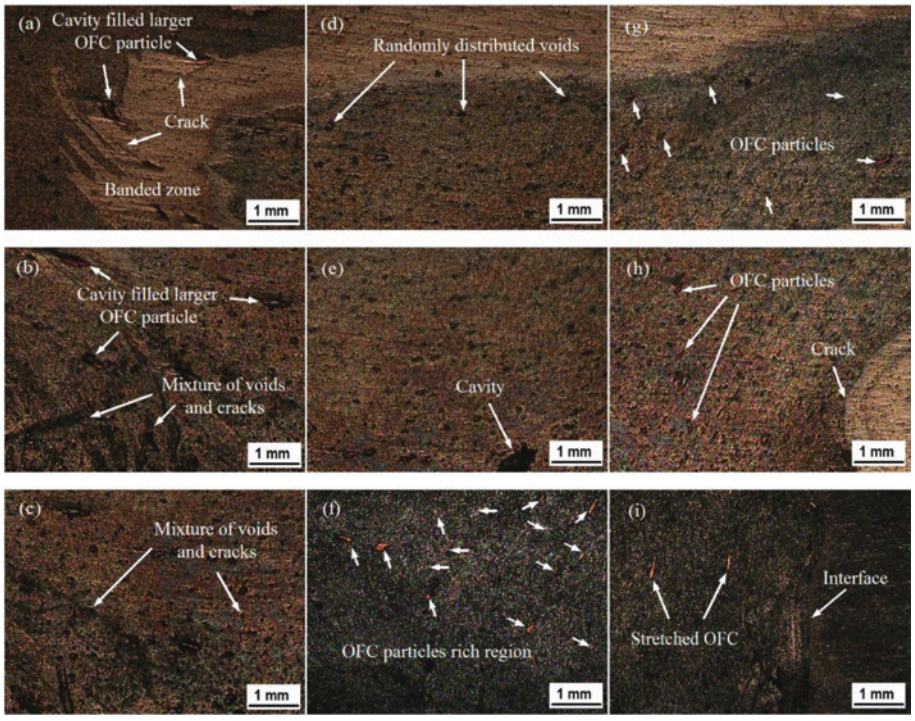

Figure 6: Optical microscope images taken from the cross section of different areas in dissimilar metal butt joints at a rotation speed of 1720 rpm. (a) to (i) Indicates sampling locations as shown in Figure 3.

distributed uniformly and sound, and defect-free welds were achieved, indicating that sound joints can be produced within the designated experimental parameters. In contrast, with a lower heat input because of a lower rotation speed, there were some voids and cracks in the nugget, and more banded structures were found. Therefore, these were not suitable to create sound welds, even though the OFC particles exhibited uniform distribution.

As mentioned above, light optical micrographs on friction-stir-welded aluminum alloys reinforced with OFC particles were observed. The microstructure change in the weld nugget was less obvious. Therefore, the OFC particle size distribution in the weld nugget could be obtained from the SEM image analysis as shown in Figure 7. The bright particles in the magnified image were identified as OFC-reinforced material, and some bright particles with a size of about several microns were uniformly distributed on top of the weld nugget and at the retreating side. Besides, it also showed the long strip-like fragmentation on the advancing side due to less stirring action.

Further analyses of the OFC particles distribution were made of the chemical composition and SEM-EDS maps (Figures 8 and 9), thus identifying the location in the weld nugget. The brighter colors indicate higher concentration of the elements, helping to observe the OFC particle distribution. Advancing and retreating sides showed distinct characteristics in the weld nuggets. Smaller particles

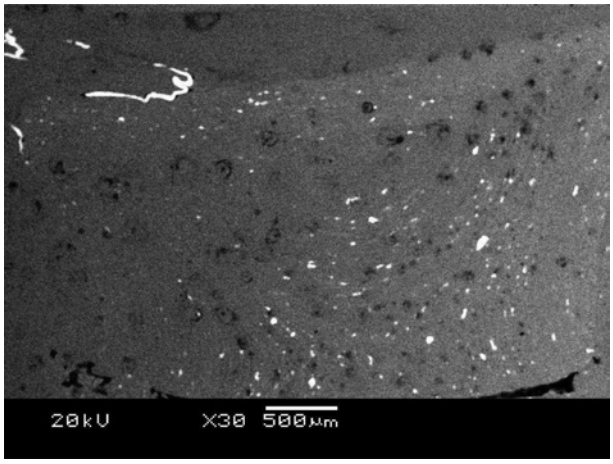

Figure 7: SEM backscattered electron image of copper particles incorporated in the nugget zone.

were uniformly distributed on the retreating side. Cu concentration was lower than outside the weld nugget. On the advancing side, light color represented high concentration of the Al element, whereas dark areas showed its absence. The large particles (approximately 20 µm) located in the dark areas were mainly composed of Cu. Larger particles (as shown in Figure 8) produced brighter Cu features, whereas smaller particles produced darker Cu features. Besides, the EDS mapping of Al in the center of the nugget zone were carried out to observe the OFC

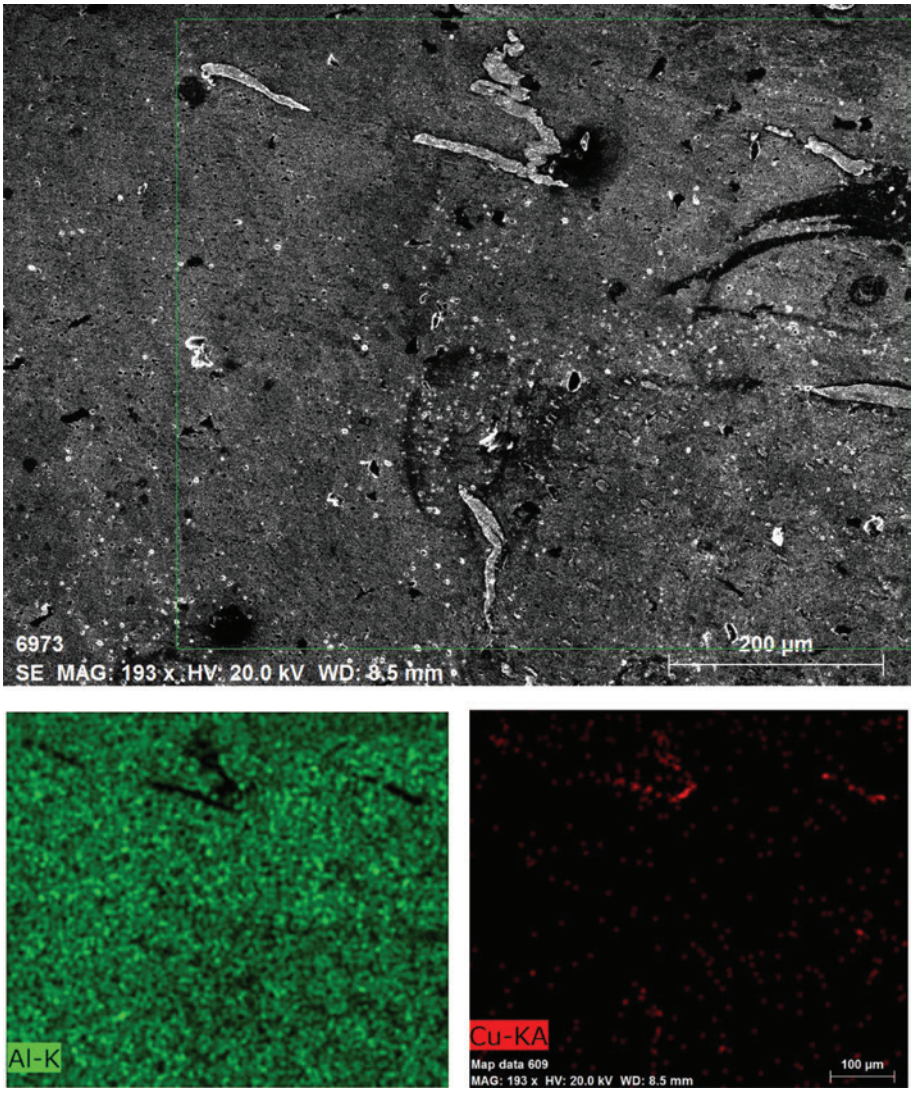

Figure 8: SEM backscattered electron image, the EDS, and the element mapping analysis on the advancing side of the stir zone.

particle distribution. Small OFC particles were observed in the dark area of the Al EDS maps. In other words, these darker areas with a green background were mainly located around the OFC particles.

The XRD diffraction patterns for the base metals and transverse cross-sectional plane of FSW joints are presented in Figure 10. The main diffraction peaks of the base metals were the α-Al phases with the (111), (200), and (311) peaks easily identified; no other phases were found. The intensity of the (111) and (200) peaks changed significantly after FSW, and the (220) planes demonstrated a tendency for preferred orientation. It also was clear that by increasing the rotation speed, the (111) and (200) peaks became stronger. Increasing the rotation speed tended to increase shear stress; therefore, grain boundary sliding occurred, which helped the grains to be oriented along the (220) plane.

3.2 Hardness tests

The hardness profile evolution between the top, middle, and bottom portions of the weld is shown in Figure 11. The zero point denotes the center of the weld nugget, and the distance from the zero indicates the interval from the measurement point to the center of the weld nugget. It is obvious that the hardness on the AA6066 side was higher than that on the AA6082 side. The average base metal microhardness could be measured at the end of both the AA6082 and AA6066 hardness profiles, and the values were approximately 52 and 64 HV, respectively. The hardness profiles in the weld nugget (produced with or without OFC reinforcement) were obviously higher than the base metals. It also became clear that the hardness of the weld nugget at the top was higher than that in the middle or bottom region. The variation in hardness from

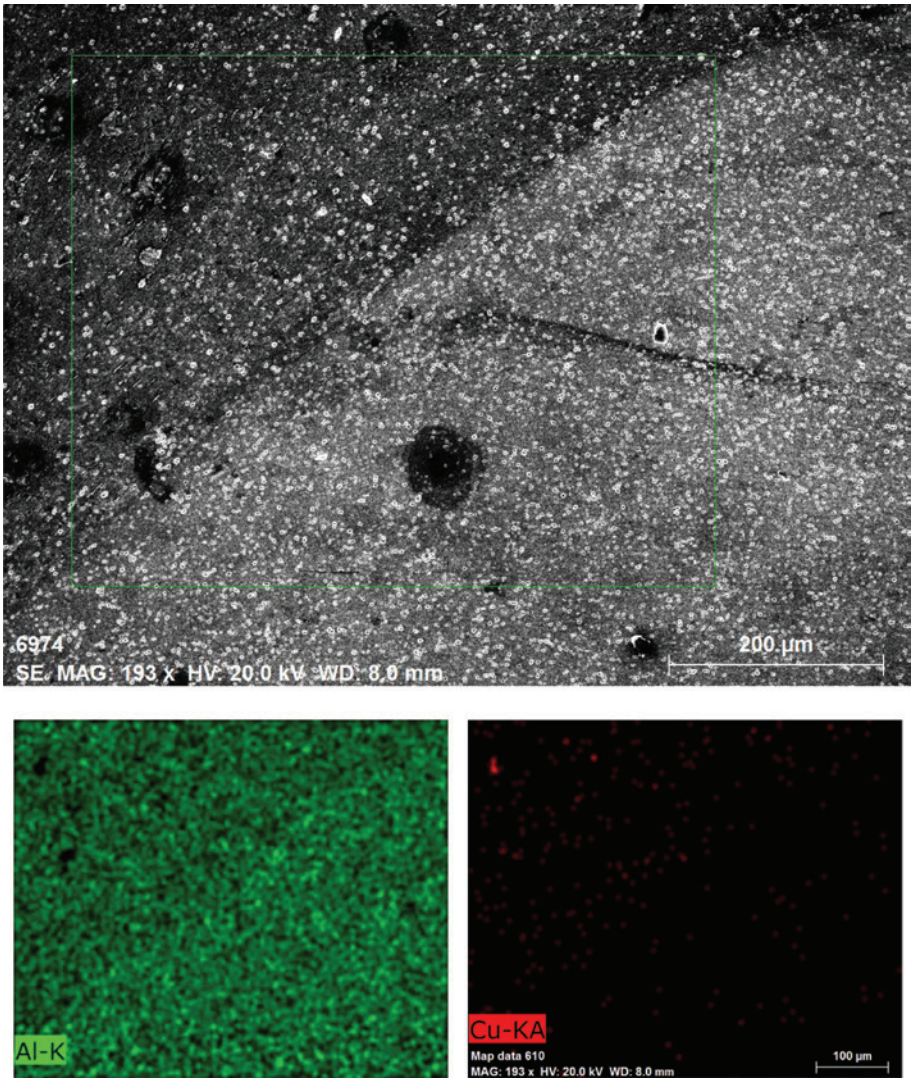

Figure 9: SEM backscattered electron image, the EDS, and the element mapping analysis on the retreating side of the stir zone.

top to bottom of the weld nugget could be attributed to grain refinement and work hardening effects. Near the top surface, closest to the tool shoulder, was subjected to greater plastic deformation compared with the material further from the tool shoulder. Conversely, the material far from the tool shoulder produced less heat input and inadequate plastic flow, therefore resulting in lower hardness.

As shown in Figure 11B, when the OFC particles were dispersed into the aluminum alloy, the hardness of the weld nugget zone significantly increased compared with that of the specimen without reinforcement. The reason may lie in the fragmentation of OFC particles giving rise to dislocation density that led to weld nugget hardening. The hardness of the unprocessed OFC used in the experiments was approximately 86 HV. The hardness distribution at the bottom line of the cross section showed higher hardness HV values than the OFC. The sharp variation of hardness in the weld nugget indicated that the OFC suffered a higher degree of strain hardening. Therefore, the hardness profiles at three positions, top, center, and bottom, exhibited significantly higher hardness.

3.3 Tensile properties and fractography analysis

Figure 12 shows the tensile stress-strain curves representing different processing conditions plotted together, including the base metals. The tensile strength and elongation of all the joints after the FSW were significantly lower than that of the base metals. This was because the tensile test samples were cut in transverse directions possibly reducing overall strength and ductility of weld joints when compared with the unwelded base metals. At

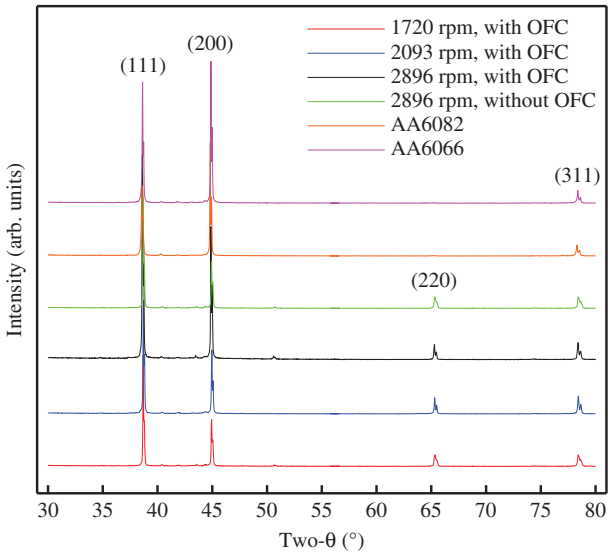

Figure 10: XRD analysis taken from the stir zone of the dissimilar metal FSW joints.

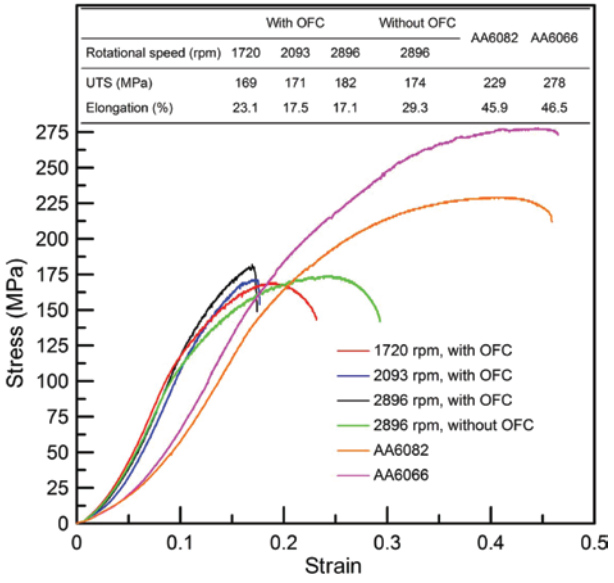

Figure 12: Tensile properties of dissimilar metal butt joints under different welding conditions.

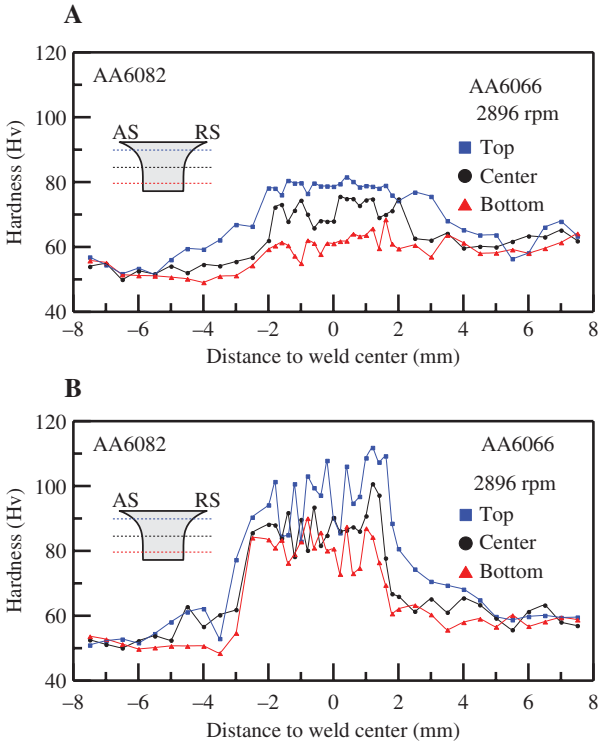

Figure 11: Microhardness profiles across the transverse cross section of welds at three different depths: (A) without reinforcing material and (B) with reinforcing material.

lower rotational speed (1720 rpm), the tensile strength of the FSW joints showed high elongation, but low tensile strength. When the rotational speed was increased, the tensile strength increased and reached a maximum at 2896 rpm. This was basically due to increased rotation speed resulting in more heat input, which could improve the flow of the plastic material and uniformly mixed the OFC reinforcement. Conversely, although rotational speed increase may have improved the tensile strength, it reduced the elongation. In the case of the FSW with OFC reinforcement, the results indicated the better rotational speed to be 2896 rpm, but its elongation value decreased by approximately 60%. As mentioned above, microstructure observations showed that the joints fabricated at lower rotational speeds (1720 and 2093 rpm) contained defects like voids or cracks in the nugget region resulting in lower tensile strength.

The fracture surfaces of the samples were studied after the tensile test by using the SEM technique. In the case of rotational speed 2896 rpm, without OFC reinforcement, the fracture surfaces showed a large number of ductile tear ridges comprising a population of microscopic shallow dimples, features reminiscent of locally ductile failure, as shown in Figure 13A,B. The SEM fracture surfaces of the FSW joint made with OFC reinforcement are shown in Figure 13C,D. Uniform circular dimples with an average size of 10 to 20 μm with slightly torn ridges, although smaller than those in Figure 13A,B, can be observed. The OFC particles caused considerable change in the behavior of the fracture process. Most of the OFC particles were firmly embedded in the matrix, as can be seen from Figure 7. At higher magnification, matrix-particle decohesion was observed (Figures 8 and 9). Therefore, the final fracture was ductile, involving the cavity

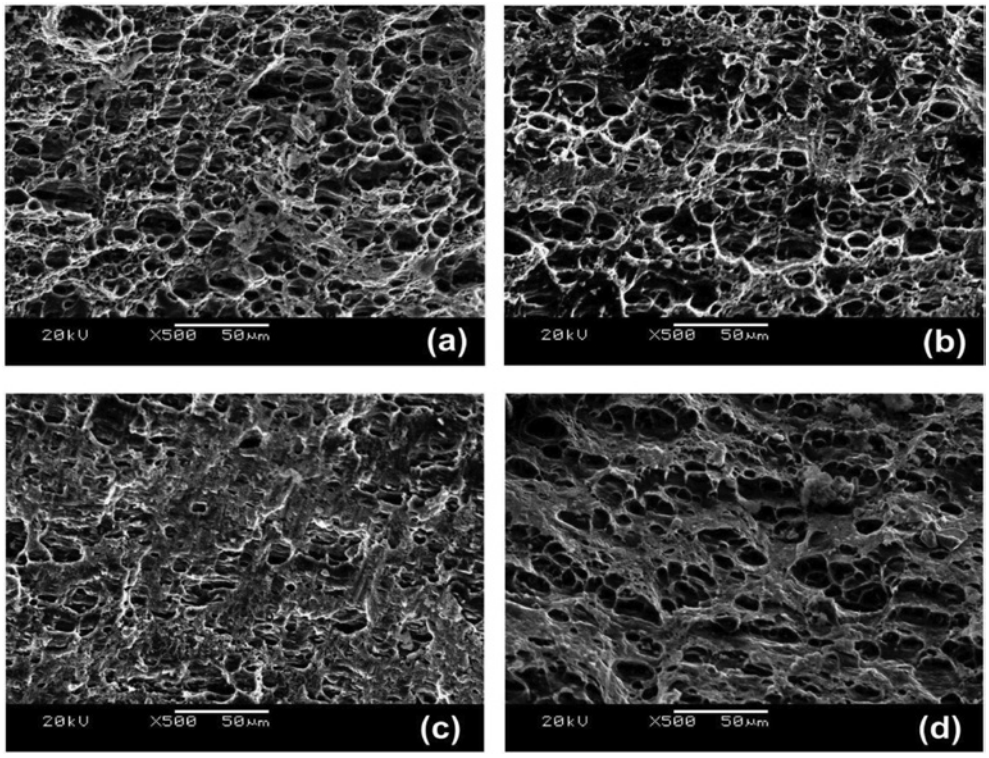

Figure 13: SEM images for the fracture surfaces in tensile tests: (a) 6082 side and (b) 6066 side without reinforcing material, (c) 6082 side and (d) 6066 side with reinforcing material.

nucleation, growth, and coalescence of voids in the matrix around the OFC particles.

4 Conclusions

1. The OFC foil provided good markers for material flow. With high-rotational-speed FSW, i.e. 2896 rpm, multilayered metal flow and formation of onion ring structures of the OFC particles were observed in the weld nuggets. The strong material flow occurred mainly on the retreating side; therefore, a uniform distribution of OFC particles was found to be clearer on the retreating side than the advancing side.
2. For a given tool traverse speed, the tool rotational speed had a significant influence on the distribution of reinforcement particles. The OFC particle size was found to be reduced with the increase of the tool rotation speed. For low tool rotation speed, typical defects such as void, cavity, and crack were evident because of the poor material mixing in the weld nugget.
3. The weld nugget hardness value was significantly higher than the base metal. The top region had the highest hardness compared with the middle and the bottom layers. As expected, it also showed higher hardness values because of the presence of the OFC particles in the weld nugget.
4. Because of the high rotation speed employed, a more homogeneous distribution of the OFC particles was achieved resulting, therefore, in weldments with high ultimate tensile strength but low ductility.
5. The XRD results indicated that the preferred orientation (220) was observed in the transverse section of the weld after the FSW. Furthermore, with increasing rotation speed, the relative intensity of the diffraction peaks (111) and (200) became stronger.

References

[1] John J, Shanmughanatan SP, Kiran MB. *Int. J. Eng. Trends Technol.* 2016, 32, 76–81.
[2] Mishra RS, Ma ZY. *Mater. Sci. Eng. R* 2005, 50, 1–78.
[3] Ilangovan M, Rajendra Boopathy S, Balasubramanian V. *Trans. Nonferrous Met. Soc. China* 2015, 25, 1080–1090.
[4] Kah P, Martikainen J. *Rev. Adv. Mater. Sci.* 2012, 30, 189–200.
[5] Dawood HI, Mohammed KS, Rajab MY. *Adv. Mater. Sci. Eng.* 2014, 2014, 1–10.
[6] Kumar HMA, Ramana VV. *Res. Inven. Int. J. Eng. Sci.* 2014, 4, 1–4.
[7] Salih OS, Ou H, Sun W, McCartney DG. *Mater. Des.* 2015, 86, 61–71.

[8] Kah P, Rajan R, Martikainen J, Suoranta R. *Int. J. Mech. Mater. Eng.* 2015, 10, 1–10.
[9] Lim DK, Shibayanagi T, Gerlich AP. *Mater. Sci. Eng. A* 2009, 507, 194–199.
[10] Morisada Y, Fujii H, Nagaoka T, Fukusumi M. *Mater. Sci. Eng. A* 2006, 419, 344–348.
[11] Lee CJ, Huang JC, Hsieh PJ. *Scr. Mater.* 2006, 54, 1415–1420.
[12] Shafiei-Zarghani A, Kashani-Bozorg SF, Zarei-Hanzaki A. *Mater. Sci. Eng. A* 2009, 500, 84–91.
[13] Guerra M, Schmidt C, McClure JC, Murr LE, Nunes AC. *Mater. Charact.* 2002, 49, 95–101.
[14] Gholami Shiri S, Sarani A, Elmi Hosseini SR, Roudini G. *J. Mater. Sci. Technol.* 2013, 29, 1091–1095.
[15] Chen SJ, Lu AL, Yang DL, Lu S, Dong JH, Dong CL. Analysis on flow pattern of bobbin tool friction stir welding for 6082 aluminum. In *Proceedings of the 1st International Joint Symposium on Joining and Welding*, Osaka, Japan, 2013, pp. 353–358.
[16] Shindo DJ, Rivera AR, Murr LE. *J. Mater. Sci.* 2002, 37, 4999–5005.
[17] Nami H, Adgi H, Sharifitabar M, Shamabadi H. *Mater. Des.* 2011, 32, 976–983.
[18] Gan YX, Solomon D, Reinbolt M. *Materials* 2010, 3, 329–350.